

27.5 A Single-Inductor AC-DC Piezoelectric Energy-Harvester/Battery-Charger IC Converting $\pm(0.35$ to $1.2V)$ to $(2.7$ to $4.5V)$

Dongwon Kwon, Gabriel Alfonso Rincon-Mora

Georgia Institute of Technology, Atlanta, GA

Microscale integration constrains energy and the lifetime microsystems like wireless sensors and biomedical implants can achieve to impractical levels. Harnessing ambient vibration energy from a small piezoelectric transducer, however, can viably keep an otherwise exhaustible battery charged. The problem is rectifying unpredictably small ac signals (which are prevalent in small volumes and with weak vibrations [1]) whose peak voltages fall below the rectified output level targeted, requires low-loss [2]–[3], no-threshold rectifiers. To fulfill these necessities, quasi-lossless LC energy-transfer networks that precede [4] or follow [5] the rectifier can extract all the energy stored in the piezoelectric capacitance and therefore overcome the basic threshold-voltage limitation, except the rectifier and its controller's headroom and quiescent current nonetheless limit the input voltage range of the system and dissipate power. The harvester-charger presented here, however, whose power-train simulation results were first reported in [6], (i) eliminates the rectifier core and its headroom limit by steering the inductor energy directly into the battery and (ii) increases the electrical damping force against which vibrations work, inducing the transducer to source more power.

Consider a lead-zirconate-titanate (PZT) cantilever generates charge as ac current i_{PZT} (Fig. 27.5.1) when stressed with a mechanical force, stores energy as it bends (in C_{PZT}), and loses leakage power (across R_{PZT}) [1]. The proposed system waits until the PZT device stores the energy vibrations produce during the positive half of vibration period T_{VIB} (5ms in Fig. 27.5.2) before engaging switches S_1 and S_N to discharge C_{PZT} into off-chip harvesting inductor L_H . The inductor current i_L rises to reach the peak, then the switches M_{P1} and S_1 de-energize L_H into the battery via i_{BAT} (Fig. 27.5.2). The system again waits for the transducer to energize C_{PZT} (in the negative direction) through the negative half of T_{VIB} (5ms) before prompting S_1 and S_N to discharge C_{PZT} into L_H , after which M_{P2} and S_N de-energize L_H into the battery.

The harvester senses when vibrations maximally charge C_{PZT} by monitoring when PZT voltage v_{PZT} peaks. The comparator CP_{PK} in Fig. 27.5.1 trips when v_{PZT} stops leading its delayed version v_D , which R_D-C_D produces. Since C_{PZT} and L_H exchange all their energy in one quarter of L_H-C_{PZT} 's resonance period (11 μ s in Fig. 27.5.2), the system predicts when C_{PZT} discharges entirely into L_H by waiting an equivalent (and tuned) delay τ_{DLY} (t_{LEN}^+ and t_{LEN}^- in Fig. 27.5.2) before de-energizing L_H . M_{P1} and M_{P2} operate as diodes because when switching voltages v_{SW}^+ and v_{SW}^- surpass V_{BAT} , comparators CP_1 and CP_2 prompt M_{P1} and M_{P2} to conduct. Conversely, when v_{SW}^+ and v_{SW}^- fall below V_{BAT} , CP_1 and CP_2 disengage M_{P1} and M_{P2} .

The harvester ultimately charges the battery from C_{PZT} by momentarily caching the energy through L_H , altogether *circumventing the input threshold voltage typical rectifiers require* to charge an output capacitor. As a result, the system can harvest from low PZT voltages, as long as the energy v_{PZT} incorporates exceeds the measured 4.62nJ/cycle the system loses as quiescent and switching power. Because the harvester completely extracts C_{PZT} 's energy before i_{PZT} has a chance to recycle it back into mechanical domain (i.e., reverse energy flow from C_{PZT} to i_{PZT}), the PZT device now generates electrical energy through out the whole period, which means the harvester increases the cantilever's electrical damping force and *induces the transducer to draw more energy*, as evidenced by the higher peak voltages the loaded PZT device generates (Fig. 27.5.2) with respect to its unloaded state. The system relies on the battery being partially charged to supply the controller circuits, whose measured headroom requires 2.5V to operate.

CP_1 and CP_2 in Fig. 27.5.1 must dissipate low power, have an ICMR that includes V_{BAT} (e.g., 2.7–4.2V for Li Ions), and respond fast enough to shut M_{P1} and M_{P2} off and block reverse current from V_{BAT} . To that end, gate-coupled differential pair $M_{PB}-M_{PD}$ in Fig. 27.5.3 compares v_{SW} with V_{BAT} and generates a proportion-

ally higher or lower current through M_{PB} , tripping output v_{CP_OUT} accordingly. L_H powers CP_1 and CP_2 and, if L_H has no energy, v_{SW} is low and M_{PD} automatically pulls v_{CP_OUT} to V_{BAT} , shutting M_{P1} and M_{P2} off while dissipating no static power. To avoid inadvertent noise-induced transitions, $M_{NH1}-M_{NH2}$ sinks a tuned current (with V_{HYST}) that unbalances the input pair and creates hysteresis when v_{SW} rises (no hysteresis exists in the falling edge because $M_{P1}-M_{P2}$ would otherwise discharge V_{BAT}). As to the rest of the system, peak-detector CP_{PK} in Fig. 27.5.1 is a conventional 55nA 2-stage comparator with a latching load to establish a $\pm 10mV$ hysteresis. For proof of concept, a $-2V$ supply (whose quiescent power measurements account) extends CP_{PK} 's ICMR to detect negative v_{PZT} 's. Tunable delay τ_{DLY} sets t_{LEN}^+ and t_{LEN}^- by slewing 2pF with adjustable current sources. Note predicting (rather than sensing) when i_L peaks avoids losing quiescent power in a current sensor.

The prototyped 2 μ m BiCMOS harvester-charger occupied 0.94 \times 0.96mm² (Fig. 27.5.7) and used an off-chip 150 μ H inductor with 2.9 Ω of equivalent series resistance. The 20M Ω -26.5pF R_D-C_D in Fig. 27.5.1 were off chip for testing flexibility. Brüel & Kjør's Mini-Shaker 4810 produced the vibrations against which the 44 \times 13 \times 0.4mm³ 290nF-5M Ω PZT cantilever (PiezoSystems, Inc.) responded and generated the corresponding v_{PZT} for the system to harvest energy.

The system harvested energy from what would have been 0.35, 0.5, 0.7, and 0.9V of unloaded PZT peak voltages to charge 160nF and 23 μ F (Fig. 27.5.4) and 1.2 and 1.5mAh Li Ions (Fig. 27.5.5). The staircase rise in V_{BAT} corresponds to the incremental energy L_H deposits at the end of each half vibration cycle. To limit the response within the targeted 2.7–4.2V Li Ion window, the capacitors in Fig. 27.5.4 were initialized to 2.7V and clamped to 4.5V with an off-chip diode and an external 4V supply.

The harvester, after discounting its losses, harnessed up to 30 μ W of output power P_{BAT} (Fig. 27.5.6) with an efficiency of 41%, peaking at 49.9% with 7.1 μ W. Since the system induces the transducer to produce more energy, loaded input power $P_{IN(LOADED)}$ peaks higher at 72 μ W than its unloaded counterpart $P_{IN(UNLOADED)}$ at 40 μ W. The corresponding rise in $P_{IN(LOADED)}$ with respect to $P_{IN(UNLOADED)}$ at 1.2V diminishes with smaller v_{PZT} 's because the increased damping force the system induces in the transducer decreases with lower input energy. The peak detector's delay compounds this drop by allowing i_{PZT} to cycle back some of C_{PZT} 's stored energy into the mechanical domain, further decreasing the damping effect. The measured efficiency (defined as the rate of P_{BAT} to $P_{IN(LOADED)}$) is lower than the simulated data in [6] because the higher C_{PZT} produced a larger inductor peak current whose adverse quadratic effects in conduction losses of the switches negated the beneficial linear effects in P_{BAT} .

Acknowledgements:

This work was funded by Linear Technology Corp. (LTC).

References:

- [1] P.D. Mitcheson, E.M. Yeatman, G.K. Rao, A.S. Holmes, and T.C. Green, "Energy Harvesting From Human and Machine Motion for Wireless Electronic Devices," *Proceedings of the IEEE*, vol. 96, no. 9, pp. 1457-1486, Sept. 2008.
- [2] T.T. Le, J. Han, A. von Jouanne, K. Mayaram, and T.S. Fiez, "Piezoelectric Micro-Power Generation Interface Circuits," *IEEE J. Solid-State Circuits*, vol. 41, no. 6, pp. 1411-1420, June 2006.
- [3] N.J. Guilar, R. Amirtharajah, and P.J. Hurst, "A Full-Wave Rectifier with Integrated Peak Selection for Multiple Electrode Piezoelectric Energy Harvesters," *IEEE J. Solid-State Circuits*, vol. 44, no.1, pp. 240-246, Jan. 2009.
- [4] Y.K. Ramadass and A.P. Chandrakasan, "An Efficient Piezoelectric Energy-Harvesting Interface Circuit Using a Bias-Flip Rectifier and Shared Inductor," *ISSCC Dig. Tech. Papers*, pp. 296-297, Feb. 2009.
- [5] S. Xu, K.D.T. Ngo, T. Nishida, G.B. Chung, and A. Sharma, "Low Frequency Pulsed Resonant Converter for Energy Harvesting," *IEEE Trans. Power Electron.*, vol. 22, no.1, pp. 63-68, Jan. 2007.
- [6] D. Kwon and G.A. Rincon-Mora, "A Rectifier-Free Piezoelectric Energy Harvester Circuit," *IEEE International Symp. Circuits and Systems*, pp. 1085-1088, May 2009.

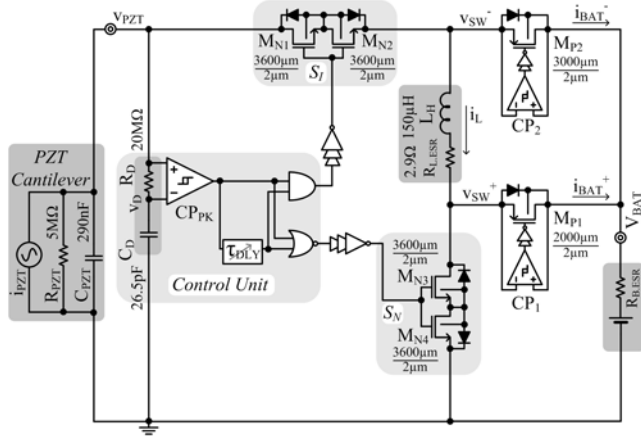


Figure 27.5.1: Prototyped piezoelectric energy-harvester/battery-charger system.

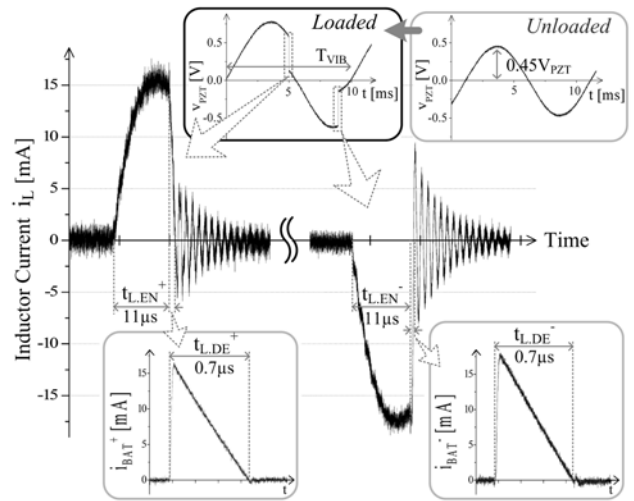


Figure 27.5.2: Experimental time-domain waveforms of PZT voltage (upper insets), inductor current, and battery currents (lower insets)

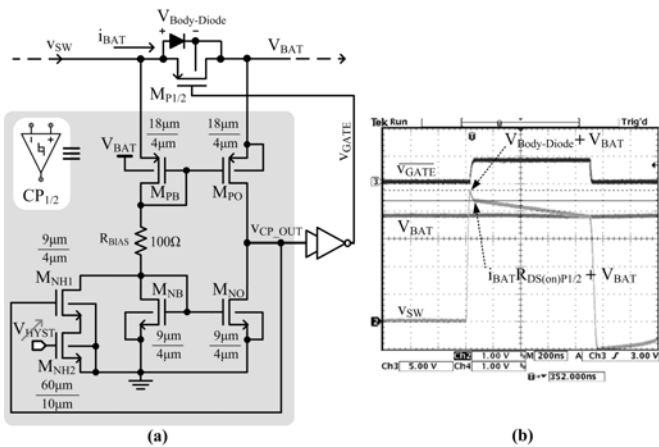


Figure 27.5.3: (a) Schematic of active-diode circuit and (b) corresponding experimental waveforms.

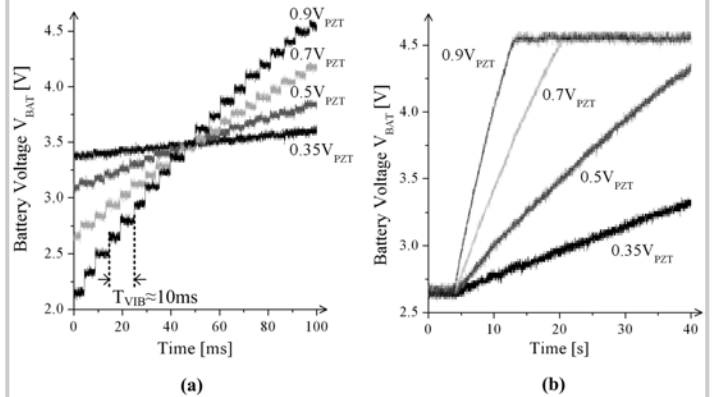


Figure 27.5.4: Measured time-domain charging profiles for (a) 160nF SMD ceramic and (b) 23µF electrolytic capacitors.

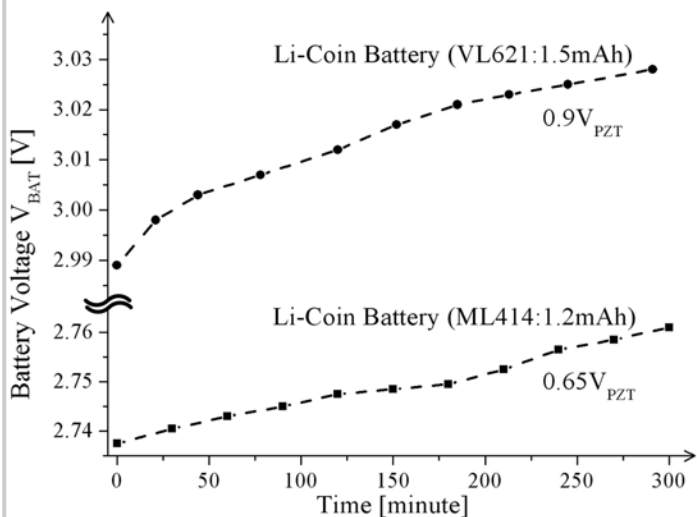


Figure 27.5.5: Experimental time-domain charging profiles for ML414 and VL621 Panasonic Li Ion coin cells.

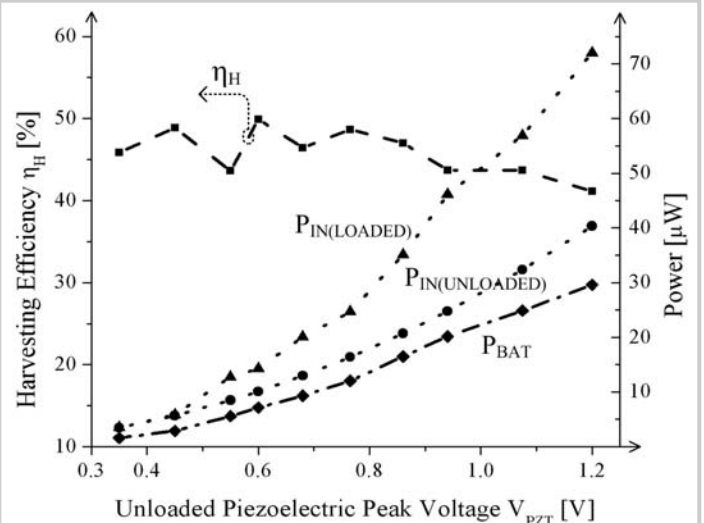


Figure 27.5.6: Measured harvesting efficiency η_H , output power P_{BAT} , and loaded and unloaded input power.

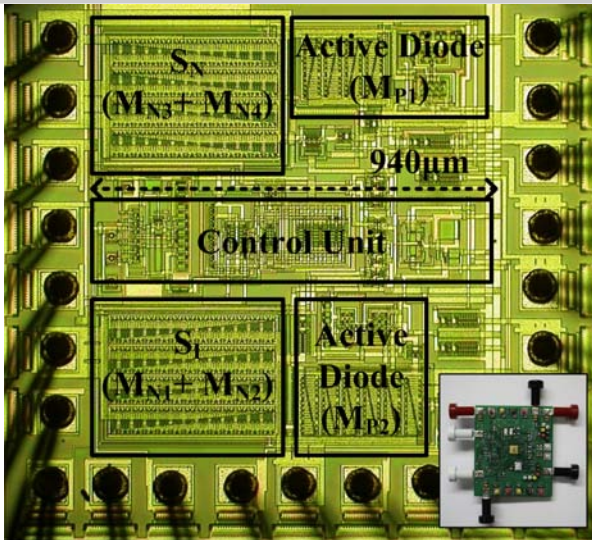


Figure 27.5.7: Die and PCB photograph of the prototyped piezoelectric energy-harvester/battery-charger system.